Activation energies for evaporation from protonated and deprotonated water clusters from mass spectra

K. Hansen,[1,a] P. U. Andersson,[2] and E. Uggerud[3]
[1]*Department of Physics, University of Gothenburg, SE-41296 Gothenburg, Sweden*
[2]*Department of Chemistry, University of Gothenburg, SE-41296 Gothenburg, Sweden*
[3]*Department of Chemistry, The Center for Theoretical and Computational Chemistry (CTCC), University of Oslo, P.O. Box 1033, Blindern, N-0315 Oslo, Norway*

(Received 6 June 2009; accepted 25 August 2009; published online 23 September 2009)

Experimental mass abundance spectra are used to extract evaporative activation energies (dissociation energies) for protonated water clusters, $(H_2O)_NH^+$, and deprotonated water clusters, $(H_2O)_NOH^-$, in the size range up to hundred molecules. The inversion is achieved by application of the shell correction method adapted from nuclear physics to the abundance spectra. The well known abundance anomaly for protonated clusters which occurs for $N=20-22$ is found to have the characteristic behavior of a shell closing, whereas other apparent magic numbers are only prominent peaks in the abundance spectra because of the instability of the evaporative precursor. For the deprotonated clusters, we find a similar shell closing for $N=55-56$. © *2009 American Institute of Physics*. [doi:10.1063/1.3230111]

I. INTRODUCTION

Water clusters play a central role in physical, chemical and biological processes of the earth and its atmosphere.[1–6] They may occur in the free form, as clathrates surrounding other molecules, or as inclusion complexes within nanocavities. Water clusters are particular relevant to the vital atmospheric processes that regulate cloud formation, and are thereby linked to the earth's radiation balance and precipitation patterns. Cloud particle development may start by the formation of water-containing clusters, but the details of this process are as of yet incompletely understood. While classical nucleation theory can be applied to larger water clusters to account for the equilibrium between evaporation and condensation, this theory may become less and less reliable as the size of the cluster becomes smaller, i.e., in the nanoscale regime.[6] Furthermore, the kinetics of evaporation/condensation of nanoscale water clusters is to a large degree affected by the presence of variable amounts of salts, organics and ions present, which makes the classical model even more uncertain.

Consequently, the quest for better knowledge of the physical and chemical properties of nanoscale clusters poses a challenge to scientists in an era where predictions of the future climate is under intense discussion. From an even more fundamental point of view, water clusters are ideal models for the condensed matter and should also be studied for this reason. The many anomalous properties of liquid water and ice are still a matter of large interest, which requires further experimental and theoretical investigation.[1]

One of the most important question that arises in this context is the stability of these clusters, in particular the binding energy of the least bound molecule. Apart from containing structural information which is of interest per se, the size dependence of the binding energy plays a crucial role in all processes related to equilibrium and quasiequilibrium abundances. It does so by determining the rate at which molecular monomers are evaporated from clusters, with its essentially exponential dependence on the activation energy.

The present study investigates the stability of positively and negatively charged pure water clusters in the size range up to hundred water molecules, probed with molecular beam experiments in vacuum. Such clusters are usually produced with broad mass distributions that reflect the kinetics of formation of the source and the specific experimental conditions used. Superposed on the broad envelope abundance distributions one observes size-to-size variations in the abundances. Such abundance anomalies were observed very early in the study of water clusters.[7–9] The cluster sizes with higher than average abundances were denoted "magic numbers," and are generally assumed to be more stable than average. Much theoretical work has been devoted to the study of the special stability of, in particular, the $N=21$ protonated water cluster.[10–12] Surprisingly, very little attention has been paid in the water cluster literature to the question of how one interprets the abundance anomalies in terms of the stability of the "magic numbers," or even if a high abundance can be ascribed to a high stability as is implicitly assumed (see, however, one attempt to quantify the effects in Ref. 13). Indeed, large abundances and high stabilities are not necessarily equivalent in molecular beam experiments. Under usually prevailing experimental conditions one can connect a high abundance with a large *change* in stability between two neighboring cluster sizes.[14] The conditions for this are that all clusters have undergone at least one evaporation and, for a quantitative analysis, that the evaporation of dimers and larger moieties is not important. Experimental studies show that metastable decay under conditions similar to those used here indeed occur via single molecule evaporation.[15–17] The condition that the clusters have undergone at least one

[a]Electronic mail: klavs@physics.gu.se.

evaporation before size selection in the mass spectrometer implies that the abundance anomalies, properly treated, are independent of the source conditions. This is a testable condition and this will be shown to be fulfilled with the data used here.

The method that will be used to analyze the experimental abundance spectra is a combination of the shell correction method and an evaporative cascade calculation. The shell correction method eliminates the broad abundance features from the data with a procedure described below. The evaporative cascade calculation relates the residual abundance variations to variations in binding energies. Evaporative ensemble considerations have been used previously[13] on measurements of metastable fractions with formulae due to Klots,[18] following an early study where patterns in metastable fractions were related to stabilities patterns.[19]

Here we consider the abundances themselves and not the metastable decay of size selected species, and we extend the study to larger sizes. If the underlying assumptions of the analysis are correct, the methods of metastable decay and abundance spectra will give identical results.

The remainder of the paper will consist of a description of the experimental apparatus used and a brief qualitative discussion of the spectra, followed by a description of the theoretical tools used in the data analysis. Finally the outcome of the analysis will be presented and discussed.

II. EXPERIMENTAL PROCEDURE

Our experimental setup consists of an electrospray ion source which produces cluster ions from pure water. After electrospraying at atmospheric pressure, the generated ions pass through two differentially pumped chambers before entering the high vacuum region of the instrument. The operating parameters of the source were optimized for production of a wide distribution of clusters. After entering the high vacuum region of the apparatus the ions are focused into the quadrupole mass filter which works as a high pass filter in these experiments. The ions are then transferred into the time-of-flight (TOF) region which is operated around 10^{-7} mbar. The TOF is of the reflectron type, and the ion beam is extracted and accelerated in a direction orthogonal to the ion optical axis by application of high voltage pulses to the acceleration electrodes. The duty cycle of the TOF is set to allow all ions in a wide mass range (strictly speaking, m/z range) to arrive before sending off the next burst of ions and the ion count rate is adjusted to allow for a sufficiently wide linear dynamic range. The mass resolution of the TOF analyzer was $m/\Delta m=5000$ (FWHM). Typically, TOF spectra are accumulated for 1–2 min for positive ions and 5 min for negative ions.

A raw data mass spectrum for the protonated clusters is shown in Fig. 1. The abundance anomalies, including the strongly enhanced peaks at m/z 379 and 505, corresponding to $(H_2O)_{21}H^+$ and $(H_2O)_{28}H^+$ have been known for a long time and interpreted in terms of increased stability of these species, as already mentioned. A spectrum of negative ions, $(H_2O)_NOH^-$, is shown in Fig. 2.

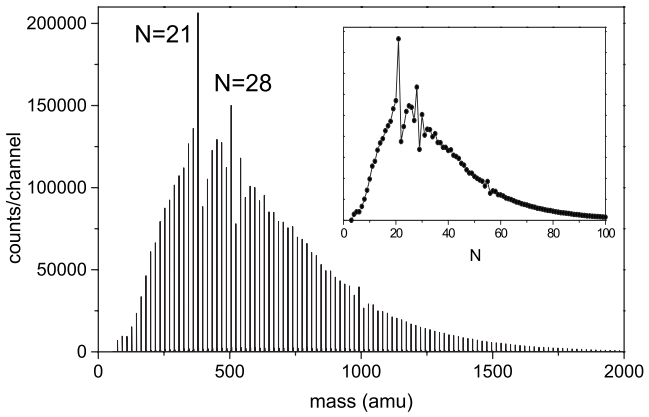

FIG. 1. Protonated water cluster mass spectrum. The inset shows the spectrum of integrated peaks of masses $1+18N$ amu.

III. DATA ANALYSIS

The conditions in the source determines the coarse features in the mass spectrum, such as mean size and width of the distribution. In addition, also the instrumental transmission and detection efficiency will in general influence the observed distribution. We have removed the global envelopes of the spectra by division with a smooth function. This procedure has been used previously[20–22] on metal and rare gas clusters, and constitute a simplified experimental application of the so-called shell correction method from nuclear physics. A rigorous derivation of the method as applied to clusters can be found in Ref. 22. The applicability of the procedure to a specific data set is best verified by comparing the reduced spectra from raw data of different experimental conditions that yield mass spectra with different global shapes.

The smooth function used here was the exponential of a fifth order polynomial where the six coefficients were fitted parameters. After division with this function the resulting spectra I_N have an average of 1 when averaged over a sufficiently wide mass range. Figures 3 and 4 show the reduced spectra. It is clear that there is a good correlation between the reduced spectra from different experimental runs for both the

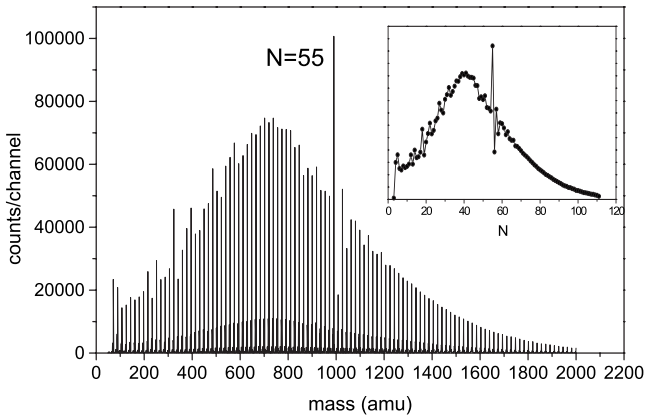

FIG. 2. Deprotonated water cluster mass spectrum. The inset shows the spectrum of integrated peaks of masses $17+18N$, corresponding to the clusters $(H_2O)_NOH^-$. The small satellite peaks are close to -2 and -3 amu below the deprotonated water clusters. They are most probable $(HO_2^-)(H_2O)_{N-1}$ and $O_2^-(H_2O)_{N-1}$.

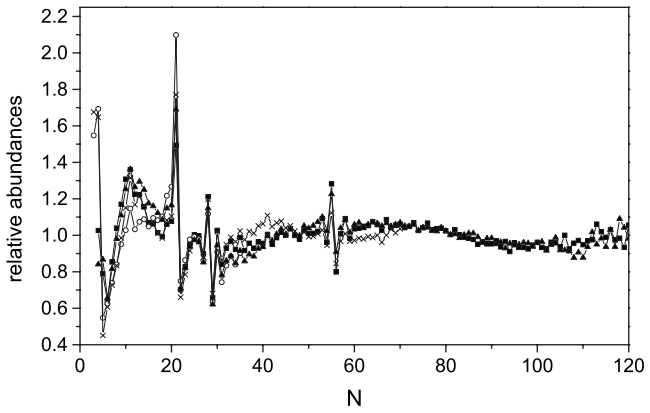

FIG. 3. Abundances of protonated water clusters after division with a smooth envelope function. The different symbols refer to different experimental runs.

positively and negatively charged clusters. The good reproducibility confirms the hypothesis that the residual structures in the spectra are generated by cluster specific properties, as opposed to the kinetics of formation or quasiequilibrium conditions in the source.

Very little structure is seen above $N \approx 70$. Some of the deviations from unity which are seen in Figs. 3 are clearly due to the inability of a fifth order polynomial to capture all variations across the mass range. In the following we only be concerned with cluster sizes up to $N=70$.

The relation between the local variations in the spectra in Figs. 3 and 4 and the relative stability of the clusters will now be established. We will make the assumption that abundances are proportional to the width of the distribution of internal energies found in the clusters at a given time. The condition that the clusters have undergone at least one evaporation before mass selection means that the energy content of the freely evaporating clusters is determined by the upper limit $E_{\max}$, which is set by the evaporative rate constant $k_N(E_{\max,N})=1/t$ together with the instrumental time t, which is the time elapsed between production of the ensemble and detection. There is a lower energy limit which is set by the corresponding higher limit for the precursor, less the loss of energy in the evaporation process, D_{N+1}, viz., $k_{N+1}(E_{\min,N}+D_{N+1})=1/t$. The time t is size dependent but it will ultimately enter into a logarithm and we can use the

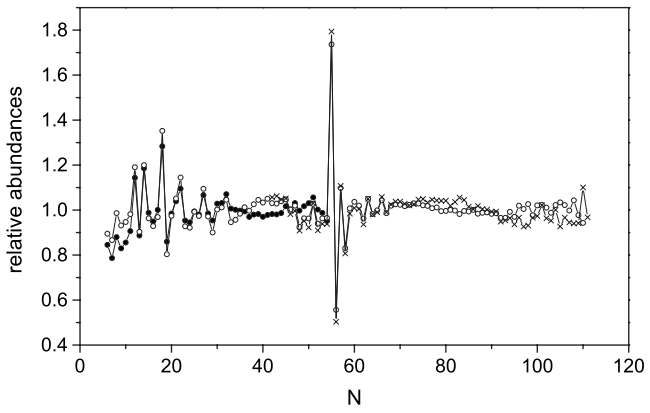

FIG. 4. Similar to Fig. 3 but for deprotonated clusters.

common value 500 μs for all sizes as a good approximation. The radiative heating time measured in ion trap experiments,[23] defined as the characteristic time needed for a cluster to absorb enough background radiation to evaporate a molecule, is given as 5 s$/N$. Our experimental time is far below this radiative heating time and radiative heating will be ignored. We can therefore identify the reduced abundance with the difference $E_{\max,N}-E_{\min,N}$, up to a constant that provides the energy scale. For a detailed derivation of results pertaining to these questions, please consult Ref. 14.

To proceed one needs an expression for the evaporation rate constant. We will use the detailed balance rate constant because this is the easiest applicable for clusters, in particular when the small fragment has rotational degrees of freedom and the transition states required for Rice-Ramsperger-Kassel-Marcus (RRKM) calculations are not known.[24] In order to calculate rate constants with detailed balance the attachment cross section for a water molecule to a cluster must be known, as must the level densities of the product and precursor, $\rho_{N-1}(E)$ and $\rho_N(E)$, i.e., the number of quantum states of the systems between the energy E and $E+dE$. The rate constant is, after integrating out the rotational motion and the translational degrees of freedom of the evaporated molecule,[24]

$$k(E) = \frac{8\pi m_{1,N-1}}{h^3}\sigma(1,N-1)T_d^2 z_{\mathrm{rot},1}\frac{\rho_{N-1}(E-D_N)}{\rho_N(E)}, \qquad (1)$$

where $m_{1,N-1}$ is the reduced mass of the evaporated molecule and the product cluster, $\sigma(1,N-1)$ is the attachment cross section for the inverse process, T_d is the microcanonical temperature of the product (daughter) cluster, defined as[25] (we will set Boltzmann's constant k_B equal to unity)

$$T_d^{-1} \equiv \frac{d\ln[\rho_{N-1}(E-D_N)]}{dE}, \qquad (2)$$

The $z_{\mathrm{rot},1}$ is the rotational partition function of the water molecule at T_d, and D_N is the dissociation energy of cluster N, defined as the difference in ground state energies E_{gs} of size $N-1$ and N

$$D_N = E_{\mathrm{gs}}(N-1) - E_{\mathrm{gs}}(N), \qquad (3)$$

where the zero of energy is chosen so that the free water molecule monomer has zero energy. It is assumed that the angular momentum of the evaporated molecule is small compared with that of the product cluster. Apart from this, the rate constant in Eq. (1) is exact. The most important feature of this expression is the ratio of level densities. For our purpose, the weakly energy dependent factor in front can be approximated with a constant because only the logarithm of it will appear. It is size dependent but also this dependence is weak enough to justify the use of a size independent value.

The cross section in Eq. (1) is calculated as the geometric attachment cross section for a cluster of bulk density and size $N=40$. The daughter temperature is summarily set to 150 K, which is a typical temperature for a 0.5 eV binding energy cluster in vacuum evaporating on our experimental time scales. The rotational partition function of the molecule

is 15.3 at that temperature, based on the known bond lengths and a symmetry factor of 2. This gives the evaporative rate constant

$$k(E) = \omega \frac{\rho_{N-1}(E - D_N)}{\rho_N(E)}, \tag{4}$$

with the frequency factor $\omega = 7.4 \times 10^{17}\ \mathrm{s}^{-1}$.

Finally, in order to solve the equation $k_N(E_{\max}) = 1/500\ \mu\mathrm{s}$ the ratio of level densities must be specified. We will first consider a form similar to the extrapolation of measured bulk thermal properties. The bulk level density is extracted from tabulated values of the heat capacity which varies close to linearly with temperature below the melting point, corresponding to a quadratic dependence of the internal energy on temperature.[26] We will correct for the degrees of freedom lost to translation and rotation by the change $N \rightarrow N-2$. Integrating gives

$$\langle E \rangle = (N-2)cT^2/2, \tag{5}$$

where c is a constant which in the bulk takes the value $2.4 \times 10^{-25}\ \mathrm{J\,K^{-2}} = 0.017\ \mathrm{K^{-1}} = 202\ \mathrm{eV^{-1}}$, as extracted from a linear fit of the bulk values of C_p.[26] This caloric curve is formally identical to that of a strongly degenerate Fermi gas and the level density associated with this system has been calculated for nuclei.[27] In the notation used here the result is

$$\rho(E) = \frac{1}{\sqrt{48E}} \exp\left(\sqrt{2(N-2)cE}\right). \tag{6}$$

This gives rate constants of

$$\begin{aligned} k_N(E) &= 7.4 \times 10^{17}\ \mathrm{s}^{-1} \frac{E}{E - D_N} \exp\left(\sqrt{2(N-3)c(E-D_N)} - \sqrt{2(N-2)cE}\right) \\ &\approx 7.4 \times 10^{17}\ \mathrm{s}^{-1} \exp\left(-D_N \sqrt{\frac{(N-2)c}{2\left(E - \frac{D_N}{2}\right)}}\right). \end{aligned} \tag{7}$$

With the condition $k(E_{\max}) = 1/t$ the maximum energy for size N then becomes

$$E_{\max,N} = \frac{D_N^2 c(N-2)}{2(\ln(\omega t))^2} + \frac{D_N}{2}, \tag{8}$$

and the energy interval spanned by the size N is

$$\begin{aligned} &E_{\max,N} - (E_{\max,N+1} - D_{N+1}) \\ &= \frac{D_N^2 c(N-2)}{2(\ln(\omega t))^2} + \frac{D_N}{2} - \left(\frac{D_{N+1}^2 c(N-1)}{2(\ln(\omega t))^2} + \frac{D_{N+1}}{2} - D_{N+1}\right). \end{aligned} \tag{9}$$

The variation in the separation energy with size is expected to be relatively small and we can linearize the difference in the quadratic terms as

$$D_N^2 - D_{N+1}^2 \approx 2\tilde{D}_N (D_N - D_{N+1}), \tag{10}$$

where $\tilde{D}_N$ is an average separation energy. The abundances then become

$$I_N \propto \frac{D_N + D_{N+1}}{2} + \frac{c(N-2)\tilde{D}_N}{\ln(\omega t)^2}(D_N - D_{N+1}) - \frac{c}{\ln(\omega t)^2}\tilde{D}_N^2, \tag{11}$$

where the separation energy in the last term has been approximated by the smooth value $\tilde{D}_N$. The constant of proportionality in Eq. (11) which was calculated in Ref. 22 to be $1/\tilde{D}_N$ changes slightly here because of the presence of the last term in Eq. (11). The value is $1/\tilde{D}_N[1 - c/\ln(\omega t)^2 \tilde{D}_N]$ (this makes the right and left hand side equal when all $D_N = \tilde{D}_N$). We then have

$$\begin{aligned} &I_N\left(1 - \frac{c}{\ln(\omega t)^2}\tilde{D}_N\right) \\ &= \frac{D_N + D_{N+1}}{2\tilde{D}_N} + \frac{c(N-2)\tilde{D}_N}{\ln(\omega t)^2}\left(\frac{D_N - D_{N+1}}{\tilde{D}_N}\right) \\ &\quad - \frac{c}{\ln(\omega t)^2}\tilde{D}_N. \end{aligned} \tag{12}$$

We note that, with Eqs. (5) and (8), we can express $c(N-2)\tilde{D}_N/\ln(\omega t)$ as the heat capacity of $E_{\max,N}$,

$$C_{v,N} = c(N-2)\tilde{D}_N/\ln(\omega t). \tag{13}$$

We therefore have

$$\begin{aligned} &I_N\left(1 - \frac{c}{\ln(\omega t)^2}\tilde{D}_N\right) \\ &= \frac{D_N + D_{N+1}}{2\tilde{D}_N} + \frac{C_{v,N}}{\ln(\omega t)}\left(\frac{D_N - D_{N+1}}{\tilde{D}_N}\right) \\ &\quad - \frac{C_{v,N}}{(N-2)\ln(\omega t)}. \end{aligned} \tag{14}$$

The analogous result for a constant heat capacity is very similar. It was derived in Ref. 14 and reads

$$I_N = \frac{D_N + D_{N+1}}{2\tilde{D}_N} + \frac{C_{v,N}}{\ln(\omega t)}\left(\frac{D_N - D_{N+1}}{\tilde{D}_N}\right). \tag{15}$$

We will use Eq. (14) because it is based on the nonharmonic bulk level density which is expected to be more realistic, but it should be stressed that only the value at the evaporative temperature is important, at least in the absence of significant entropic effects and the results will therefore not depend critically on the variation in the heat capacity with temperature. The heat capacities can be extracted from measurements of metastable decay fractions because these are proportional to the heat capacity when the evaporation time is short.[28] Measurements of heat capacities for protonated water clusters and water clusters with an anionic core, of sizes from 5 to 300 (Ref. 29) have been performed and

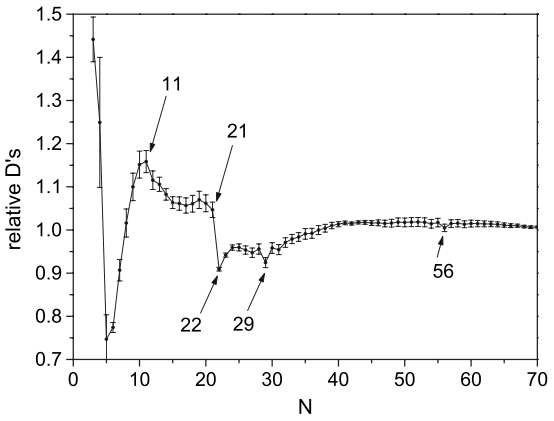

FIG. 5. Relative dissociation energies of protonated water clusters derived from abundance spectra and Eq. (14).

gave similar values for anionic and cationic clusters. The values were found to be reasonably well represented by the equation

$$C_{v,N} = 7.8(N-2), \tag{16}$$

which is higher than the bulk ice heat capacity at 150 K. This temperature can be used as reference temperature based on the liquid drop energies and evaporative ensemble results (see below). The trend to a higher heat capacity than bulk at these temperatures has also been seen in direct measurements of a few medium size cationic water clusters.[30] We have used the value 7.8 in the analysis throughout. The uncertainty is typically 10%. An overall reduction in $C_{v,N}$ changes the amplitude of the variations in binding energies around the average upwards with a similar relative amount, and vice versa for a reduction.

IV. RESULTS AND DISCUSSION

The result of the inversion of the experimental data with Eq. (14) is shown in Figs. 5 and 6. Individual spectra are inverted and averages and uncertainties are then calculated for each mass separately, based on the data provided by the inverted spectra. We note that the relatively large amplitude of the abundance variations around $N=55$ for the negative clusters translates into a small amplitude in the variation in the dissociation energies. This is a consequence of the heat capacity that appears as a constant of proportionality in the equation that links the two quantities. The notion that high relative abundances does not necessarily reflect high absolute stability, but is due to a stability change, is seen particularly clearly for the protonated cluster where the minor $N=55$ abundance peak is caused by a slightly *reduced* stability of the $N=56$ cluster. On the other hand, the protonated cluster around $N=21$ display the signatures of a shell closing, with the characteristic slowly varying value below the shell closing, followed by a sudden drop at the shell closing. The anionic clusters display a similar shell closing at $N=55$. This is somewhat surprising in the light of the qualitative similarity between the structures at $N=55-56$ of the two charge states. Numerically, the explanation is that the structure at $N=54$ and $N=57-58$ differ for the two charge states. For the protonated clusters, some structure may also be hidden in the uncertainties which must be considered an upper limit of the true values.

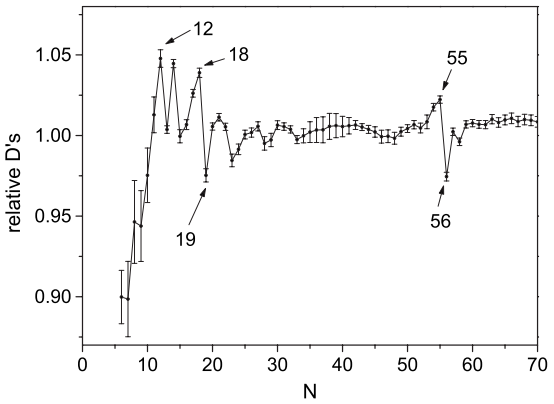

FIG. 6. Relative dissociation energies of deprotonated water clusters derived from abundance spectra and Eq. (14).

The analysis so far has been made in terms of relative energies. A determination of absolute values require that an absolute energy scale is introduced. We will use the liquid drop parameters for a charged spherical water droplet for this purpose. The liquid drop, or Thomson liquid drop model, parameterizes the energy of a cluster in powers of the reciprocal cuberoot of N which, for a constant density, corresponds to an expansion in reciprocal powers of the radius. The parameters are the bulk dissociation energy, surface tension and charging energy. By construction, it does not include structural anomalies and the associated energy variations in specific cluster sizes. For considerations of chemical equilibrium it is conveniently formulated in terms differences in Gibbs' free energies.[31] However, for the present purpose ground state properties are more appropriate because the level density is parameterized from the ground state. The expression reads[29]

$$\tilde{D}_N = A - \frac{2}{3}BN^{-1/3} + \frac{1}{2}\frac{e^2}{4\pi\varepsilon_0}\left(1-\frac{1}{K}\right)\frac{1}{3r_1}. \tag{17}$$

The parameter $A=0.49$ eV is the bulk binding energy per molecule,[29,32] i.e., the zero temperature enthalpy, $B=4\pi r_1^2\sigma = 0.22$ eV is proportional to the surface tension σ and surface area as indicated (the liquid water 0 °C surface tension is used). The "molecular radius" r_1 is defined such that the bulk reciprocal molecular density is equal to $4\pi r_1^3/3$. The parameters of the third term are the standard electrostatic ones, where the relative dielectric constant K is so large that $1/K$ can be ignored in the expression. This gives us

$$\tilde{D}_N = 0.49\ \text{eV} - 0.22\ \text{eV}\ N^{-1/3} + 1.25\ \text{eV}\ N^{-4/3}. \tag{18}$$

The expression has a shallow minimum around $N=23$ and increases strongly below. These liquid drop values have been multiplied with the D_N's shown in Figs. 5 and 6 and the result is shown in Figs. 7 and 8. The parameters are extrapolations from bulk and we stress that it is highly nontrivial that they are valid over the huge span in sizes from macroscopic water to the smallest water clusters. There is a surprisingly good agreement between our values and those based on equilibrium experiments in the figures for the re-

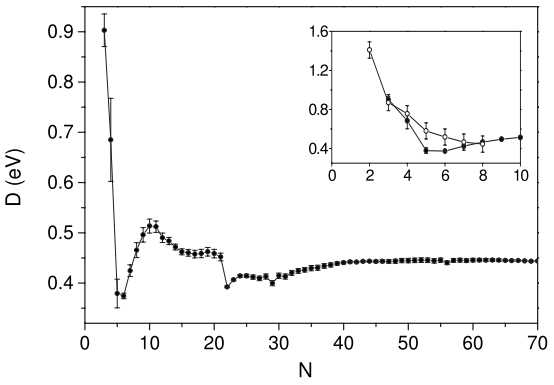

FIG. 7. The dissociation energies for protonated water clusters, extracted from abundance spectra and scaled with the liquid drop model described in the text. The inset shows the comparison between our results up to $N=10$ (filled circles) and average values of literature enthalpies of dissociation determined under near equilibrium conditions (open circles) (Refs. 33–36).

gion with overlapping measurements, $N=3-8$ for the protonated and for $N=6-7$ for deprotonated clusters.

The anions and cations have a significantly different behavior for small sizes. The shell correction procedure does not allow strong conclusions to be made about the few points closest to the extremes of the spectrum. This fact is reflected in the uncertainties which are determined from the scatter of data points from individual spectra. We have at present no explanation for the differences between the negatively and positively charged clusters.

The analysis here involve ground state separation energies. These enter in a natural way because of the chosen parameterization of the level densities, as seen from the derivation. A number of other functional forms of the level density versus energy will also give ground state energies, although it is not a general rule. We will defer further discussion of these questions until more experimental evidence is available, except for a comment on the "latency effect." The effect is the observation that the 'magic' nature of $N=21$ and $N=28$ appears long time after ionization, on time scales of $4-40$ μs.[37] This effect is interpreted, correctly we believe, as a solidification of the clusters that appears when evaporative processes have cooled the clusters sufficiently. This means that the protonated cluster separation energy D_{21} extracted here is most likely the difference between the free energies of two clusters in different phases, liquid-like for $N=22$ and solidlike for $N=21$. This changes the interpretation but does not invalidate our derivation of the abundance-energy relation in Eq. (14). We should emphasize that it is not possible with the present data and analysis alone to conclude anything about the phase of the clusters.

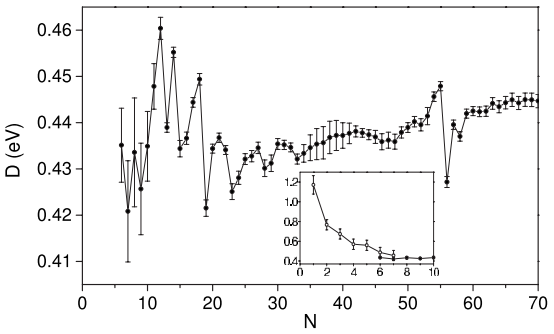

FIG. 8. Similar data as in Fig. 7 but for deprotonated water clusters. Note the relatively weak tendency to divergence for small cluster sizes relative to the positive clusters. The liquid drop energies are identical in the two cases.

The dissociation energies found here should be compared with literature data. There are several studies, both experimental and theoretical that show that the dissociation energy drops in the range $N=1-5$.[12,13,33–35,38,39] However, the existing literature data are inconclusive regarding the situation for $N>5$. In some cases the experimental uncertainties are also too large to assess any trend. To our knowledge there exist only two data sets covering the whole range 1–30. Shi *et al.*[13] applied Klot's evaporative model to determine dissociation energies from metastable $(H_2O)_NH^+$ ion decay curves. They found a minimum for D but at a value of $N=10$ which is above our minimum (see Fig. 7). Their curve is rather featureless with no particular stability variation at $N=21$. The absence of this is ascribed by the authors to entropic effects. From the low energy CID study of Magnera *et al.*[38] a minimum was found at $N=8$. We note that our curve in Fig. 7 has a local maximum at $N=10$. For higher values of N, Magnera *et al.*[38] find that the value of D are almost constant, with the exception of a peak value at $N=21$. This peak appears isolated, in contrast to our data, where the $N=21$ is the edge of a high binding plateau extending to lower sizes. We do not wish to draw strong conclusions from the comparisons with the data of Shi *et al.*[13] and Magnera *et al.*[38] for different reasons. For the former, the experimental data consisted in metastable fractions that are related to the ratio of two consecutive dissociation energies. The D_N's for the whole region are then found by multiplication of all ratios. The numerical stability of such a procedure which involves a so-called telescoping series has, to our knowledge, not been verified in the literature. For the latter, the data were analyzed without inclusion of the kinetic shift, whereas this is an essential part of the analysis of the present experiments, cf., Equation (8). The results of the data processing cannot therefore be expected to agree in the two cases.

Two photon absorption experiments provide other interesting comparisons. In Ref. 40, the average dissociation energies around $(H_2O)_N$, $N=18,34$ are determined to 0.43 and 0.44 eV, respectively. This is very close to the values found for the same sizes of the slightly different anions studied here, corroborating the liquid drop parameterization. In another study, of a cationic water cluster with a dopand of a single aniline molecule and ten water monomners,[41] a similar technique as used in Ref. 40 gives a dissociation energy of 0.46–0.51 eV. Also this is very close to the values found here around $N=10$. Obviously, the very good agreement may be fortuitous, but it should be kept in mind that dissociation energies are differential binding energies and can be less sensitive to the nature of a core molecule than total binding energies.

Finally, we note that except for providing unique insight into cluster structure as discussed above, the new data presented here are particularly significant to ionic condensation processes in the atmosphere.[42]

V. SUMMARY

The dissociative activation energies for positively and negatively charged water clusters have been determined for cluster sizes between 5 and 120, with an inversion of mass abundance spectra. The spectra have been treated with a procedure that extracts the binding energies and at the same time allows a check of the assumptions used in this part of the analysis. The expected special features in the thermal properties of water clusters was found to have very little effect on the inversion procedure, indicating that the procedure is robust. The well known structures at $N=21-22$ for the positive clusters and $N=55-56$ for the negative show the shape typical of shell closings, whereas the minor structure at $N=55-56$ in positive clusters is due to a reduced stability of $N=56$. Between $N=70$ and $N=120$ very little structure is seen in either charge state.

ACKNOWLEDGMENTS

This work was supported by the Swedish National Research Council (VR) by grants to KH and PUA, the Nanoparticle in Interactive Environments platform at the faculty of science at Gothenburg University, and by the Norwegian Research Council. Valuable comments from O. Echt and B. Dynefors are gratefully acknowledged. Thanks are due to J. Vedde, O. Sekiguchi, and M. J. Ryding for experimental assistance.

[1] M. F. Chaplin, Water Structure and Behaviour (2008) (http://www.lsbu.ac.uk/water/), with 1572 references (as of May, 2009).
[2] *Biophysics of Water*, edited by F. Franks and S. Mathias (Wiley, London, 1982).
[3] A. A. Konsta, J. Laudat, and P. Pissis, Solid State Ionics **97**, 97 (1997).
[4] S. Y. Lo, W. C. Li, and S. H. Huang, Med. Hypotheses **54**, 948 (2000).
[5] I. Brovchenko, A. Krukau, A. Oleinikova, and A. K. Mazur, J. Phys. Chem. B **111**, 3258 (2007).
[6] A. Laaksonen, V. Talanquer, and D. W. Oxtoby, Annu. Rev. Phys. Chem. **46**, 489 (1995).
[7] S.-S. Lin, Rev. Sci. Instrum. **44**, 516 (1973).
[8] J. Q. Searcy and J. B. Fenn, J. Chem. Phys. **61**, 5282 (1974).
[9] J. L. Kassner, Jr. and D. E. Hagen, J. Chem. Phys. **64**, 1860 (1976).
[10] A. Khan, Chem. Phys. Lett. **319**, 440 (2000).
[11] S. S. Iyengar, M. K. Petersen, T. J. F. Day, C. J. Burnham, and V. E. Teige, J. Chem. Phys. **123**, 084309 (2005).
[12] M. P. Hodges and D. J. Wales, Chem. Phys. Lett. **324**, 279 (2000).
[13] Z. Shi, J. V. Ford, S. Wei, and A. W. Castleman, Jr., J. Chem. Phys. **99**, 8009 (1993).
[14] K. Hansen and U. Näher, Phys. Rev. A **60**, 1240 (1999).
[15] P. Scheier and T. D. Märk, Phys. Rev. Lett. **59**, 1813 (1987).
[16] C. E. Román and I. L. Garzón, Z. Phys. D: At., Mol. Clusters **20**, 163 (1991).
[17] P. U. Andersson, M. J. Ryding, O. Sekiguchi, and E. Uggerud, Phys. Chem. Chem. Phys. **10**, 6127 (2008).
[18] C. E. Klots, Z. Phys. D: At., Mol. Clusters **21**, 335 (1991).
[19] A. J. Stace and C. Moore, Chem. Phys. Lett. **96**, 80 (1983).
[20] J. Borggreen, K. Hansen, F. Chandezon, T. Døssing, M. Elhajal, and O. Echt, Phys. Rev. A **62**, 013202 (2000).
[21] L. Schweikhard, K. Hansen, A. Herlert, M. D. Herráiz Lablanca, and M. Vogel, Eur. Phys. J. D **36**, 179 (2005).
[22] S. Prasalovich, K. Hansen, M. Kjellberg, V. Popok, and E. E. B. Campbell, J. Chem. Phys. **123**, 084317 (2005).
[23] T. Schindler, C. Berg, G. Niedner-Schatteburg, and V. Bondybey, Chem. Phys. Lett. **250**, 301 (1996).
[24] K. Hansen, Philos. Mag. B **79**, 1413 (1999).
[25] J. U. Andersen, E. Bonderup, and K. Hansen, J. Chem. Phys. **114**, 6518 (2001).
[26] *CRC Handbook of Chemistry and Physics*, edited by D. R. Lide, 89th ed. (CRC Press/Taylor and Francis, Boca Raton, 2009), Internet Version.
[27] A. Bohr and B. R. Mottelson, *Nuclear Structure* (World Scientific, Singapore, 1998).
[28] C. E. Klots, Z. Phys. D: At., Mol. Clusters **5**, 83 (1987).
[29] A. E. K. Sundén, K. Støchkel, S. Panja, U. Kadhane, P. Hvelplund, S. Brøndsted Nielsen, H. Zettergren, B. Dynefors, and K. Hansen, J. Chem. Phys. **130**, 224308 (2009).
[30] C. Hock, M. Schmidt, R. Kuhnen, C. Bartels, L. Ma, H. Haberland, and B. v. Issendorff, Phys. Rev. Lett. **103**, 073401 (2009).
[31] W. A. Donald and E. R. Williams, J. Phys. Chem. A **112**, 3515 (2008).
[32] *CRC Handbook of Chemistry and Physics*, edited by R. C. Weast, 58th ed. (CRC Press, Cleveland, 1978).
[33] A. J. Cunningham, J. D. Payzant, and P. Kebarle, J. Am. Chem. Soc. **94**, 7627 (1972).
[34] Y. K. Lau, S. Ikuta, and P. Kebarle, J. Am. Chem. Soc. **104**, 1462 (1982).
[35] M. Meot-Ner and C. V. Speller, J. Phys. Chem. **90**, 6616 (1986).
[36] NIST Chemistry WebBook, NIST Standard Reference Database Number 69 (http://webbook.nist.gov/chemistry/).
[37] O. Echt, D. Kreisle, M. Knapp, and E. Recknagel, Chem. Phys. Lett. **108**, 401 (1984).
[38] T. F. Magnera, D. E. David, and J. Michl, Chem. Phys. Lett. **182**, 363 (1991).
[39] T. Wróblewski, L. Ziemczonek, E. Gazda, and G. P. Karwasz, Radiat. Phys. Chem. **68**, 313 (2003).
[40] P. J. Campagnola, L. A. Posey, and M. A. Johnson, J. Chem. Phys. **95**, 7998 (1991).
[41] A. H. Nam, H. S. Park, M. A. Lee, N. R. Cheong, J. K. Song, and S. M. Park, J. Chem. Phys. **126**, 224302 (2007).
[42] N. Marsh and H. Svensmark, Phys. Rev. Lett. **85**, 5004 (2000).